SUPPORTING INFORMATION

Antiangiogenic Effect of Dual/Selective $\alpha_5\beta_1/\alpha_v\beta_3$ Integrin Antagonists Designed on Partially Modified Retro-Inverso Cyclotetrapeptide Mimetics.

Luca Gentilucci,[a] Giuliana Cardillo,[†,a] Santi Spampinato[§,b] Alessandra Tolomelli,[a] Federico Squassabia,[c] Rossella De Marco,[a] Andrea Bedini,[b] Monica Baiula,[b] Laura Belvisi.[d,††] Monica Civera[d]*

[a] Department of Chemistry "G. Ciamician", Università degli Studi di Bologna, via Selmi 2, 40126 Bologna, Italy.

[b] Dept. of Pharmacology, Università degli Studi di Bologna, via Irnerio 48, 40126 Bologna, Italy.

[c] Stepbio srl, Bologna, Via P. Nanni Costa 12/3/e - 12/3/f - 40133 Bologna.

[d] Dept of Organic and Industrial Chemistry, and Centre for biomolecular Interdipartimental Studies and Industrial applications (CISI),University of Milano, Via Venezian 21, Milano.

* e-mail: luca.gentilucci@unibo.it; phone: +39 0512099462; fax: +39 0512099456

† e-mail: giuliana.cardillo@ciam.unibo.it;

§ e-mail: santi.spampinato@unibo.it;

†† e-mail: laura.belvisi@unimi.it

Table of contents

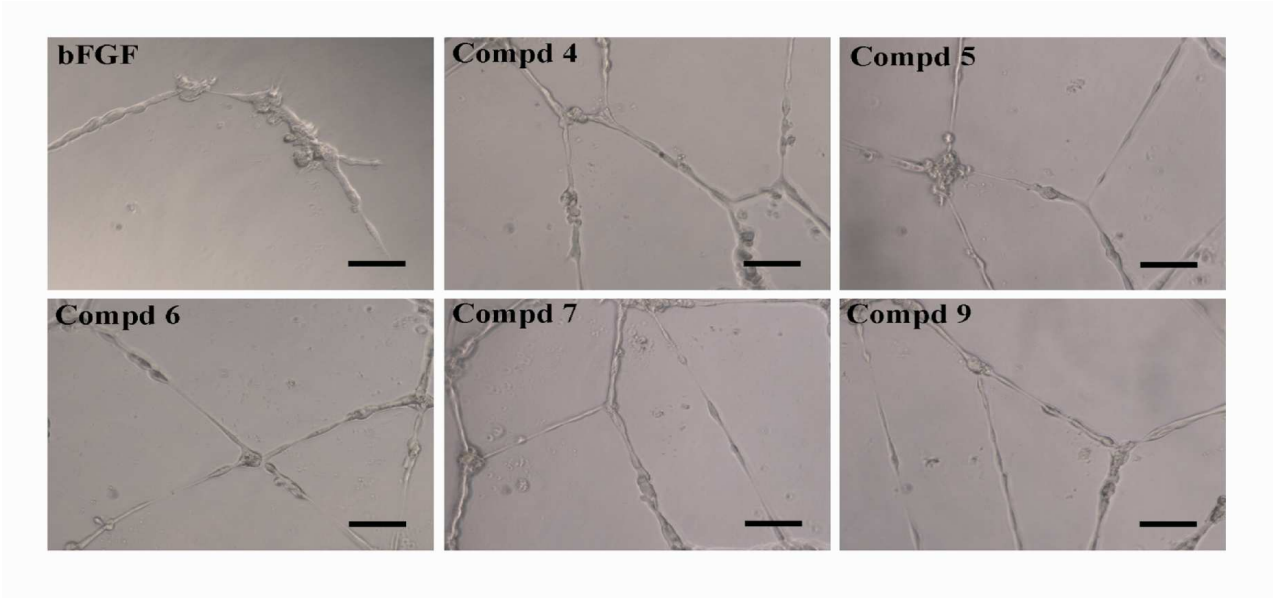

Figure S1. Tube formation of HUVEC cells on Matrigel. Representative pictures of capillary-like structures (black bar in the pictures corresponds to 100 μm). HUVEC cells were treated with or without integrin antagonists (10 μM) and then plated on Matrigel in the absence or presence of bFGF (30 ng/mL) for 16h. Compounds **4**, **5, 6, 7** and **9** were not effective as angiogenesis inhibitors.

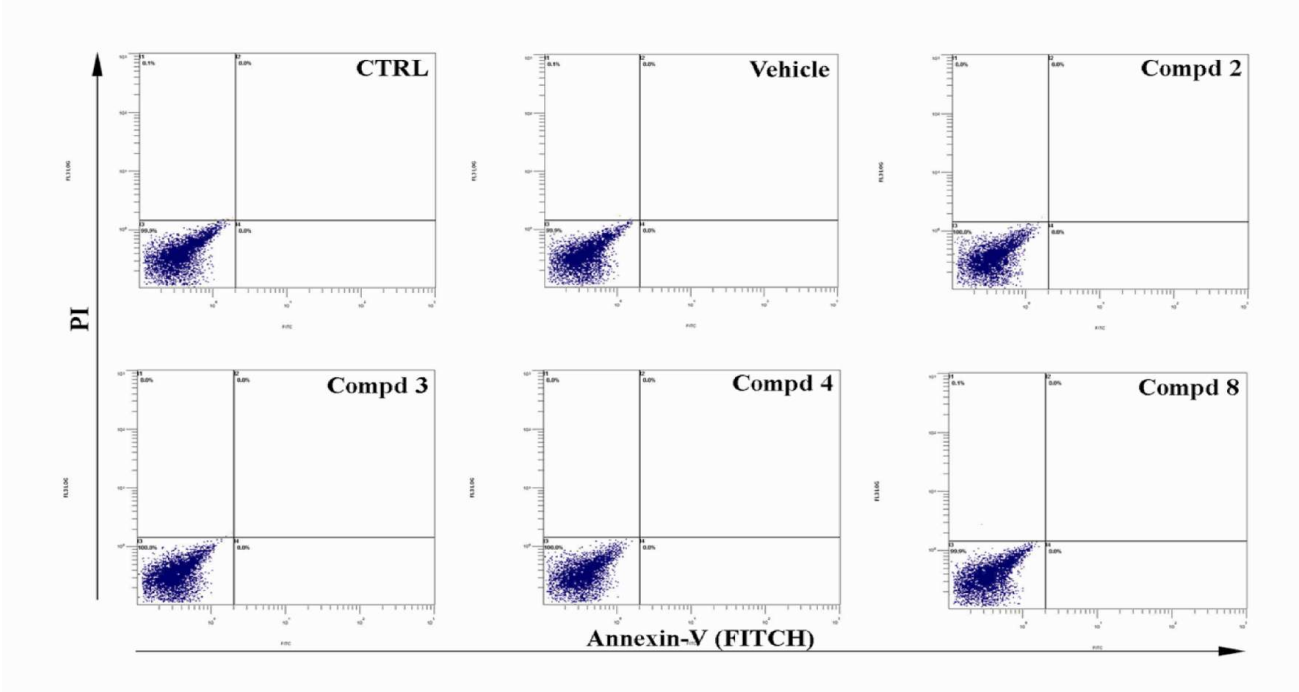

Figure S2. $\alpha_v\beta_3/\alpha_5\beta_1$ integrin antagonists did not induce apoptosis or necrosis in endothelial cells. No significant increase in apoptotic or necrotic cells was observed among endothelial cells treated with 10 μM integrin antagonists. HUVEC cells were treated with integrin antagonists for 16 h; then the cells were detached and stained with Annexin-V and PI to distinguish healthy cells (Annexin-V^- and PI^-), early apoptotic cells (Annexin-V^+ and PI^-), and late apoptotic/necrotic cells (Annexin-V^+ and PI^+). A representative experiment of three done with superimposable results is shown.

Analytical characterization of PMRI RGD-mimetics 4, 5.

Compounds **6-9** are the enantiomers of **2-5**, respectively. The syntheses of **3-9** were performed as reported for **2**.

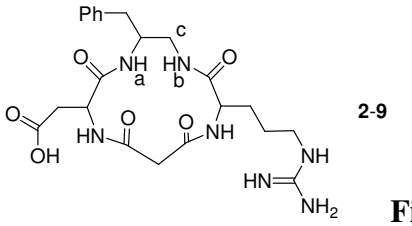

2-9

Figure S3

(**4**), c[βPheψ(NHCO)Aspψ(NHCO)Gly-(*R*)-Arg]. ^{1}H-NMR (400 MHz, 8/2 DMSO-d_6/H_2O): δ = 1.40-1.55 (m, 3H, ArgHγ+ArgHβ), 1.67 (m, 1H, ArgHβ), 2.36 (dd, J= 9.0, 15.0 Hz, 1H, AspHβ), 2.50 (dd, J= 4.0, 15.0 Hz, 1H, AspHβ), 2.58-2.87 (m, 3H, Hc+diamHβ), 2.91 (d, J= 10.4 Hz, 1H, $COCH_2CO$), 2.92-3.20 (m, 2H, ArgHδ), 3.20 (d, J= 10.4 Hz, 1H, $COCH_2CO$), 3.55 (m, 1H, Hc), 3.80 (m, 1H, diamHα), 3.90 (m, 1H, ArgHα), 4.18 (m, 1H, AspHα), 6.65 (d, J= 8.4 Hz, 1H, NHa), 6.95 (br.t, 1H, NHb), 7.10-7.35 (m, 5H, ArH), 8.00 (br.s, 1H, ArgNHε), 8.61 (br.d, 1H, ArgNH), 8.75 (br.d, 1H, AspNH). ^{13}C-NMR (400 MHz, 8/2 DMSO-d_6/H_2O): δ = 27.0, 30.2, 36.0, 37.4, 38.5, 40.0, 40.6, 48.2, 49.9, 51.4, 55.3, 125.1, 128.0, 128.3, 129.0, 129.2, 138.2, 163.6, 171.8, 173.2, 173.5, 175.0, 176.5.

(**5**), c[βPheψ(NHCO)-(*R*)-Aspψ(NHCO)Gly-Arg]. ^{1}H-NMR (400 MHz, 8/2 DMSO-d_6/H_2O): δ = 1.38-1.57 (m, 3H, ArgHγ+ArgHβ), 1.61 (m, 1H, ArgHβ), 2.41 (dd, J= 9.0, 15.0 Hz, 1H, AspHβ), 2.54 (dd, J= 4.0, 15.0 Hz, 1H, AspHβ), 2.70-2.80 (m, 2H, diamHβ), 2.81 (d, J= 10.6 Hz, 1H, $COCH_2CO$), 2.90 (m, 1H, Hc), 2.91-3.19 (m, 2H, ArgHδ), 3.22 (d, J= 10.4 Hz, 1H, $COCH_2CO$), 3.50 (m, 1H, Hc), 3.90 (m, 1H, diamHα), 4.05 (m, 1H, ArgHα), 4.25 (m, 1H, AspHα), 6.99 (d, J= 8.4 Hz, 1H, NHa), 7.08 (br.t, 1H, NHb), 7.10-7.38 (m, 5H, ArH), 8.30 (br.s, 1H, ArgNHε), 8.40 (br.d, 1H, ArgNH), 8.75 (br.d, 1H, AspNH). ^{13}C-NMR (400 MHz, 8/2 DMSO-d_6/H_2O): δ = 26.7, 30.6, 36.9, 37.3, 38.4, 39.8, 40.4, 48.8, 49.7, 52.3, 55.3, 125.7, 128.2, 128.8, 129.4, 129.6, 135.2, 164.6, 169.8, 173.7, 174.0, 175.6, 176.4.

Table S1. Non-obvious ROESY cross-peaks observed for **4**. Stereochemistry has been omitted. For Ha, Hb, Hc, see Figure S3; u = upfield, d = downfield; vs = very strong, s = strong, m = medium, w = weak

Cross peak	Intensity	Cross peak	Intensity
AspNH-NHa	s	AspNH-ArgNH	w
AspNH-AspHα	m	AspNH-$COCH_2CO_u$	vs
ArgNH-$COCH_2CO_u$	s	AspNH-$COCH_2CO_d$	w
ArgNH-$COCH_2CO_d$	m	AspNH-Asp$H\beta_d$	w

NHb-ArgHα	s	ArgNH-NHb	s
NHa-NHb	m	ArgNH-ArgHα	s
diamHα-NHb	m	ArgNH-NHa	w
NHb-Hc_u	m	NHb-Hc_d	vs
NHa-diamHβ	s	NHa-Asp$Hβ_d$	m
NHa-Hc_u	w	NHa-AspHα	m
AspHα-Asp$Hβ_d$	m	AspHα-Asp$Hβ_u$	w
ArgHα-Arg$Hβ_u$	vs	NHa-diamHα	s
ArgHα-Arg$Hβ_d$	m	diamHα-diamHβ	s
ArgHα-ArgHγ	w	ArgHα-ArgHδ	m
diamHα-Hc_u	m	diamHα-Hc_d	vs
diamHα-diamHβ	vs	Hc_u-diamHβ	s
Hc_u-diamHβ	m	ArgHδ-ArgHγ	s
ArgHβ-ArgHγ	vs		

Table S2. Non-obvious ROESY cross-peaks observed for **5**. Stereochemistry has been omitted. For Ha, Hb, Hc, see Figure S3; u = upfield, d = downfield; vs = very strong, s = strong, m = medium, w = weak

Cross peak	Intensity	Cross peak	Intensity
AspNH-Asp$Hβ_d$	m	AspNH-$COCH_2CO_d$	m
AspNH-AspHα	s	AspNH-NHa	s
AspNH-$COCH_2CO_u$	s	ArgNH-$COCH_2CO_u$	vs
ArgNH-ArgHα	m	ArgNH-NHb	s
ArgNH-Arg$Hβ_d$	m	NHb-Hc_d	s
NHb-diamHβ	w	NHb-diamHα	w
NHb-ArgHα	vs	NHb-ArgNH	vs
NHb-Hc_u	m	NHa-diamHβ	s
NHa-Hc_d	m	NHa-diamHα	s
AspHα-Asp$Hβ_d$	m	AspHα-Asp$Hβ_u$	w
NHa-AspHα	vs	NHa-ArgHα	w
diamArH-Hc_d	m	diamArH-diamHβ	vs
diamArH-diamHα	vs	diamArH-AspHα	w
ArgHα-Arg$Hβ_d$	m	diamArH-Hc_u	m
ArgHα-ArgHγ	w	ArgHα-ArgHδ	m
diamHα-diamHβ	vs	ArgHα-Arg$Hβ_u$	s
diamHα-Hc_u	s	diamHα-Hc_d	m
ArgHβ-ArgHγ	s	ArgHδ-ArgHγ	s

*Conformational analysis of **4** and **5** in solution.*

The conformational analyses of **4** and **5** were performed by NMR spectroscopy and Molecular Dynamics (MD) simulations as reported for **2**, **3**. The ^{1}H-NMR of **4** and **5** revealed a single set of resonances. Variable temperature ^{1}H-NMR experiments were utilized to deduce the presence of H-bonds involving amide protons (Table S3).

Table S3. Δδ/Δt values (ppb/°K) of amide protons for **4** and **5**, determined by VT-^{1}H-NMR analysis in 8/2 DMSO-d_6/H_2O at 400 MHz over the range 298-348 °K. (NHa, NHb, see Figure S3)

Compd	AspNH	ArgNH	NHa	NHb
4	-4.0	-3.0	-1.3	-0.2
5	-2.8	-3.0	-0.7	-1.5

As for **2**, in **4** and **5** the comparatively low Δδ/Δt values of diamine NHa and NHb with respect to AspNH and ArgNH suggest the existence of secondary structures in equilibrium, alternatively stabilized by H-bonds involving NHa or NHb.

Molecular backbone conformations were investigated by 2D ROESY and restrained molecular dynamics performed in a box of explicit water. For the absence of $H\alpha_i$-$H\alpha_{i+1}$ cross peaks, all of the ω bonds were set at 180°. After cluster analysis, for both **4** and **5** the computations essentially gave two kinds of structures, **4a/4b** (Figure S4) and **5a/5b** (Figure S5), differing exclusively by the opposite orientation of ArgNH, and AspNH, respectively, each showing some constraint violations (Table S4).

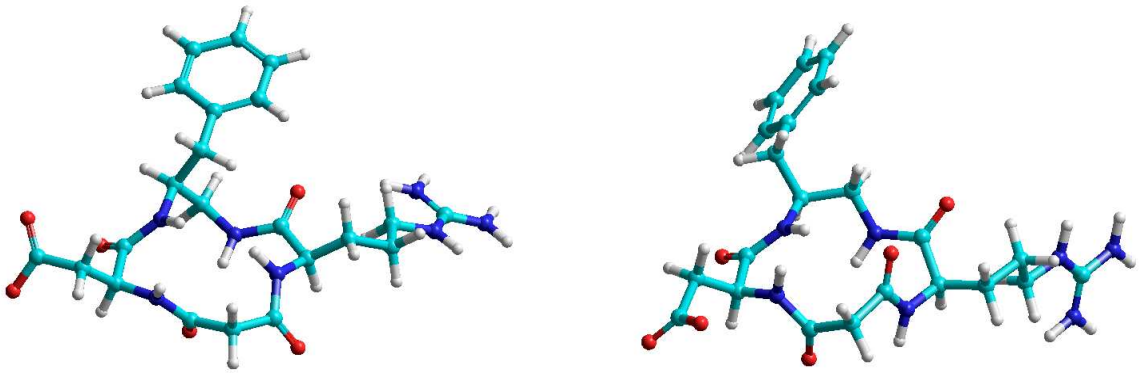

Figure S4. Representative, low-energy structure **4a** (left) and **4b** (right) consistent with ROESY analysis.

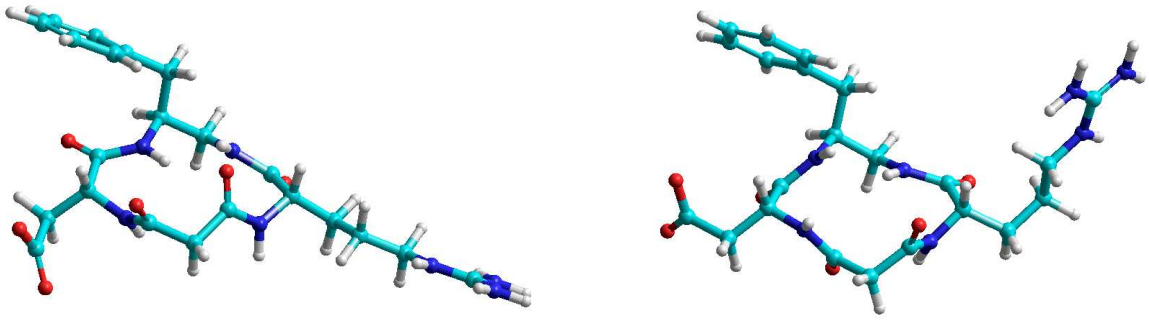

Figure S5. Representative, low-energy structure **5a** (left) and **5b** (right) consistent with ROESY analysis.

The couples **4a/4b** and **5a/5b** reasonably represent conformers in equilibrium. The structure **4a** is compatible with the strong cross-peaks observed between $COCH_2CO_u$ and both AspNH and ArgNH; the structure **4b** is compatible with the medium cross peak between $COCH_2CO_d$ and ArgNH, and with the strong cross-peak between ArgNH and ArgHα. For compound **5**, the strong cross peaks between $COCH_2CO_u$ and both AspNH and ArgNH account for the structure **5a**; the cross peak of medium intensity between AspNH and $COCH_2CO_d$, and the strong cross-peak between AspNH and AspHα account for the structure **5b**.

The structures **4b** and **5b** show a smaller number of distance violations (Table S4) with respect to **4a** and **5a**, respectively, and conformations more compatible with VT-NMR data, which are suggestive of H-bonds on both NHa and NHb.

Table S4. Distance violations, calculated vs constraint (Å)[a] for ROESY-derived structures. Residue stereochemistry has been omitted.

4a	**4b**	**5a**	**5b**
ArgNH-ArgHα	ArgNH-ArgHα	AspNH-AspHα	AspNH-AspHα
2.9 vs 2.6	2.3 vs 2.6	2.9 vs 2.6	2.3 vs 2.6
ArgNH-NHb		AspNH-NHa	
2.9 vs 2.6		2.9 vs 2.6	
ArgNH-$COCH_2CO_u$	ArgNH-$COCH_2CO_u$	AspNH-$COCH_2CO_u$	AspNH-$COCH_2CO_u$
2.3 vs 2.6	3.5 vs 2.6	2.3 vs 2.6	3.5 vs 2.6
ArgNH-$COCH_2CO_d$		AspNH-$COCH_2CO_d$	
3.5 vs 2.9		3.5 vs 2.9	

[a] The authors are aware that being concerned about distance differences that are a few tenths of an Angstrom different could be misleading in this context.

During the unrestrained MD in explicit solvent performed on **4a**, **4b**, **5a**, and **5b**, the analysis of the trajectories revealed the presence of H-bonded structures involving NHa and/or NHb (not

shown), as suggested by VT-NMR data. The simulations failed to reproduce the inversion of ArgNH for **4**, and the inversion of AspNH for **5**; evidently, these rotations are slow compared to the time selected for the simulation.

The compounds **6**-**9** were not investigated; their structures were generated as the mirror mages of the respective enantiomers **2**-**5**.

The comparison of the in-solution structures of **2** and **3** with the structures of **4**-**9**, and the correlation with their experimental affinity for $\alpha_5\beta_1$ and $\alpha_v\beta_3$ integrins give several clues to discuss the interaction with the receptors.

Compounds **4**, **5**, **8**, and **9**, show a cis disposition of Asp and Arg (Figure S4 and S5 and respective mirror images). The analysis of the trajectories of unrestrained molecular dynamics confirms that the average distance between the pharmacophores is shorter with respect to the distance considered optimal for binding $\alpha_5\beta_1$ and $\alpha_v\beta_3$ integrins.

In **4**, the guanidino group of (R)-Arg is placed on the opposite side of the cyclic scaffold with respect to **2**, **3** (see the main text). Apparently, the long and flexible side chain of Arg still allows a certain interaction with the receptors. In the preferred conformation **4b**, the benzyl side chain of the diamine points below the molecular plane, as for **2**, but the pseudo-equatorial position seems scarcely effective in discriminating the different sizes/shapes of the lipophilic pockets of the $\alpha_v\beta_3$ (small pocket) or $\alpha_5\beta_1$ (large pocket) receptors. This situation is consistent with a moderate affinity towards both the receptors, in the micromole range, with no selectivity.

While in **4** the carboxylic group of Asp points towards the receptor's cation in a straight line, as in **2** and **3**, in **5** the carboxylic group of (R)-Asp is placed on the opposite side of the cyclic scaffold. This difference accounts for the lack of activity of **5**.

Compound **6** and **7** are the enantiomers of **2** and **3**, respectively, and the same distance between the pharmacophores can be observed (the conformational analysis was not repeated). This distance matches the one required for a good interaction with the receptors. However, as for **5**, the D-Asp residue places the carboxylic group on the opposite side of the scaffold respect to the compounds **2**-**4**. As a consequence, **6** and **7** seem to be scarcely adapt to interact the receptors.

In contrast, compound **8** shows a moderate experimental affinity for both $\alpha_5\beta_1$ and $\alpha_v\beta_3$ integrins despite of the presence of (R)-Asp. Besides, the complete lack of activity of **9** towards both the $\alpha_v\beta_3$ and $\alpha_5\beta_1$ receptors remains for the moment elusive. Further insight can be obtained for the $\alpha_V\beta_3$ integrin by molecular docking.

*Molecular docking of **4**-**9**.*

In order to rationalize, on a molecular basis, the affinity of the compounds for the $\alpha_v\beta_3$ receptor, docking studies were performed following the same virtual screening protocol used for compounds **2** and **3**. Ligands **4** and **8** produced top-ranked poses conserving all the important interactions of the X-ray complex (Figure S6) with the benzyl side chain of the diamine pointing toward the outside of the integrin binding site, allowing the aromatic ring to fit unhindered. In the calculated docking poses, compound **4** fits the receptor by reproducing the RGD backbone of the X-ray ligand better than the conformations of ligand **8** (Figure S6). Altogether these computational findings agree with the comparable micromolar activity observed for **2**, **3, 4** and **8** for the integrin $\alpha_v\beta_3$.

On the contrary, most poses generated by the automated docking calculations for the inactive compounds **5**, **6**, **7** and **9** failed in forming all the key ligand-protein interactions, as revealed by the less favourable Glide score values. The stereochemistry array of the residues in compounds **5**, **6**, **7** and **9** produce three-dimensional pharmacophoric arrangements forcing the entire molecule to enter the receptor lopsided. In particular, the electrostatic interactions drive the fit of these ligands into the receptor binding site, but cause the loss of the complex network of hydrogen bonds. Especially, the presence of a (R)-Asp residue seems to hamper the proper fit of the ligands in the receptor cleft (see **5**, **6**, **7**).

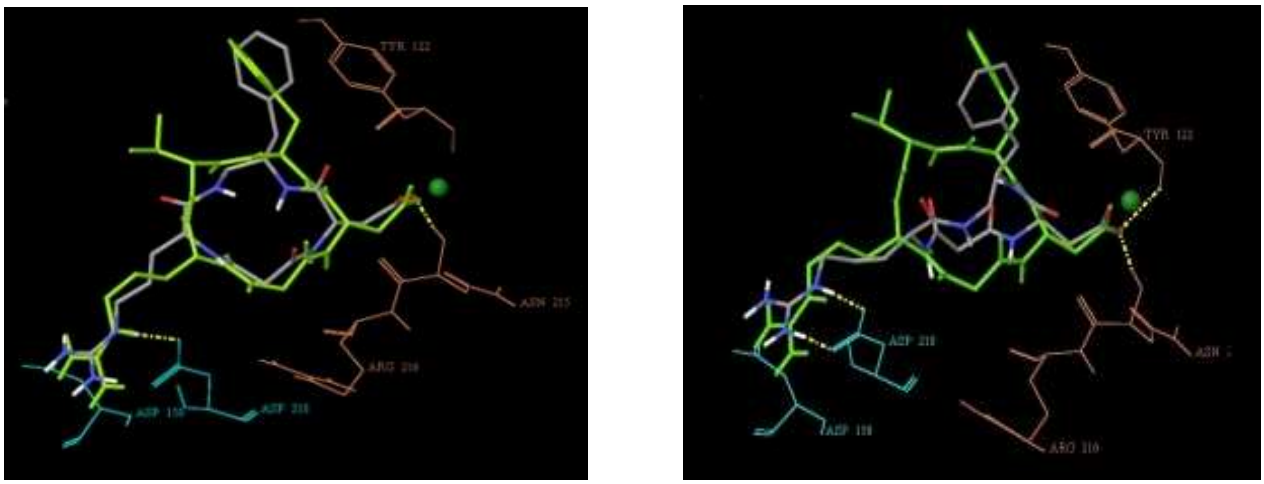

Figure S6. Top-ranked docking poses of ligands **4** (left side) and **8** (right side) (atom colour tube representation) into the crystal structure of the extracellular domain of $\alpha_V\beta_3$ integrin (α unit cyan and β unit orange wire representation) overlaid on the bound conformation of cilengitide (green tube representation). Only selected integrin residues involved in the interactions with cilengitide are shown. The Mn^{2+} ion at MIDAS is shown as a green CPK sphere. Nonpolar hydrogen atoms were removed for clarity.

In conclusion, the conformational analyses and molecular docking computations of **2**-**9** confirm that the distance between the pharmacophores is the primary requisite for a correct interaction with the receptors, as expected, but this feature has no effect on selectivity. Data explain the experimental observation that the presence of (S)-Asp and (S)-Arg is a pre-requisite to obtain the highest affinity. The presence of (R)-Arg can be tolerated, due to the flexibility of its side chain, while the presence of (R)-Asp is generally deleterious for activity. The only exception is **8**, which likely adopts an alternative receptor-bound conformation (calculated only for $\alpha_V\beta_3$ integrin).

In the proposed model, the disposition of the benzyl group of the diamine plays a fundamental role in selectivity. It is possible to perceive that a pseudo-equatorial orientation of the benzyl group is well tolerated by both $\alpha_5\beta_1$ and $\alpha_V\beta_3$ integrins. Interestingly, compound **2,** the only compound with a well precise axial disposition of the benzyl, is also the only compound selective for $\alpha_5\beta_1$ over $\alpha_V\beta_3$ integrin.